Comparison of the finite strain macroscopic behavior and local damage of a soft matrix highly reinforced by spherical or polyhedral particles

Foucault de Francqueville [a,b], Pierre Gilormini [c], Julie Diani [a,*], Aude Vandenbroucke [b]

[a] Laboratoire de Mécanique des Solides, CNRS UMR 7649, École Polytechnique, Institut Polytechnique de Paris, Route de Saclay, 91128, Palaiseau, France
[b] ArianeGroup, Centre de recherche du Bouchet, 9 rue Lavoisier, 91710, Vert-le-Petit, France
[c] Laboratoire PIMM, ENSAM, CNRS, CNAM, Hesam Université, 151 bd de l'Hôpital, 75013, Paris, France

ARTICLE INFO

Keywords:
Polyhedral particles
Damage
Non-linear behavior
Finite elements
Micromechanics

ABSTRACT

Motivated by the different uniaxial responses of two actual materials filled with either sifted glass beads or sifted glass grits, the influence of the fillers shape on the finite strain behavior of highly filled composites (>50%) is examined through micromechanical finite element simulations accounting for matrix/filler debonding with a cohesive-zone model. Three-dimensional matrix cells filled with 64 monosized spherical particles are compared to cells filled with the same number of monosized polyhedra. For this purpose, an original generation process was developed to obtain periodic cells with random dispersions of non-regular polyhedra. Finite element simulations of uniaxial tensile tests on the periodic cells allow studying the influence of the fillers shape on the macroscopic behavior and on the local damage at the matrix/filler interfaces. Actually, the presence of sharp edges and apexes for polyhedral particles seems to have a second order impact compared to the cohesive-zone parameters. The damage fields demonstrate the same trends for both particles shapes. The different behaviors observed on actual composites are rather due to different adhesion properties between fillers and matrix than to the shape of particles.

1. Introduction

In an attempt to develop solid propellants delivering always more power, new highly energetic fillers have been introduced in the soft constituent matrix material, with undesired poor consequences on the strength and toughness of the composite. These unsatisfactory mechanical properties may be attributed to either the change of the matrix/filler adhesion due to the different nature of the fillers or the more faceted shape of the new fillers since particle size and aspect ratios have been kept similar. The current contribution explores the impact of the presence of vertices, edges and faces at the surface of polyhedral particles, on the mechanical stress-strain response of highly reinforced particulate soft materials undergoing possible damage at the matrix/filler interfaces. The typical material of interest is a soft matrix filled with randomly dispersed quasi-rigid monosized inclusions reaching a volume fraction of 55%. For this purpose, a model soft rubber-like matrix was filled with either glass grits or glass beads and tested in uniaxial tension until failure to characterize the mechanical responses.

Previously three-dimensional numerical representations and mechanical simulations of such composites with interfacial damage dealt mostly with ductile matrices moderately filled with spherical fillers (see for instance Llorca and Segurado, 2004; Segurado and Llorca, 2005 among others), and fewer studies account for more realistic polyhedral fillers (Williams et al., 2012; Weng et al., 2019). Numerical studies considering composites with an hyperelastic matrix for which, unlike ductile matrix, the softening is due to the damage at the matrix/filler only and a very large stiffness contrast exists between the constitutive phases, are mostly two-dimensional (Moraleda et al., 2009; Toulemonde et al., 2016; Zhang et al., 2018; Li et al., 2018) with little three-dimensional contributions (Gilormini et al., 2017), all considering spherical particles. The most common generation process for obtaining microstructures filled with irregular polyhedra is based on random sequential additions (Widom, 1966) of identical (Böhm and Rasool, 2016; Drach et al., 2016) or different (Lavergne et al., 2015; Sheng et al., 2016) polyhedra. However, like for monosized spherical inclusions, the process is limited to volume fractions well bellow 55%. Other approaches consisting in the division of space using Poisson planes or Voronoï tessellation followed by the shrinkage of the polyhedra faces in order to obtain the targeted volume fraction of particles are better suited for our application. Such a microstructure building process has been

* Corresponding author.
E-mail address: julie.diani@polytechnique.edu (J. Diani).

used for the simulations of concrete (Carol et al., 2007; Caballero et al., 2006), metal matrix composites (Fritzen and Boehlke, 2011), asphalt (Wimmer et al., 2016) or solid propellants (Nadot-Martin et al., 2011). Numerical simulations of the mechanical properties of such composites are usually based on periodic cells combined with periodic boundary conditions that allow reducing the size of the representative volume element (RVE) (Kanit et al., 2003) to a reasonable extent. Account for matrix debonding at matrix/filler interfaces, as it has been observed experimentally (Cornwell and Schapery, 1975; Oberth and Bruenner, 1982; Gilormini et al., 2017) is then possible using finite element analysis (FEA) with cohesive-zone models (CZM) that may be implemented rather simply (Segurado et llorca 2005; Inglis et al., 2007; Gilormini et al., 2017). The objective here is to run such simulations with faceted particles and compare the computed macroscopic behavior and microscopic damage with those obtained for the same soft matrix reinforced by spherical particles.

The paper is organized as follows. In the next section, the experimental evidences motivating the study are reported in terms of the microstructures and mechanical behaviors of model materials consisting of an acrylate soft matrix filled with different glass fillers. Section 3 presents the numerical materials and simulation framework. Then, results of the finite strain uniaxial tension simulations are reported discussing the link between the local damage and the resulting macroscopic mechanical responses for both composites filled with spherical glass beads or polyhedral glass fillers. Concluding remarks close the paper.

2. Microstructure and behavior of actual model composites

Model particulate reinforced materials have been elaborated in the lab. A rubbery polymer matrix network has been highly filled with 200/250 μm sifted glass beads or slivers. The matrix was synthesized by mixing 98% molar mass of methacrylate (MA) and 2% molar mass of polyethylene glycol dimethacrylate (PEGDMA) of molar weight 750 g/mol, with photo-initiator 2,2-Dimethoxy-2-phenylacetophenone (DMPA). The products were used as received by Sigma-Aldrich. The fillers were first cleaned following Cras et al. (1999) recommendations and slowly added to the stirring mix. The pasty blends were poured in glass molds and exposed to UV light during 40 min for polymer cross-linking. Once removed from the molds, the composite plates were exposed to a temperature of 45°C during 15 min for annealing possible process residual stresses. The material microstructures recorded with microCT scans are displayed in Fig. 1. The fillers are of similar sizes and the glass slivers aspect ratios, while not being equal to 1, remain close to 1.

For mechanical testing, rectangular specimens of final dimensions 40 $\times$ 10 $\times$ 3 mm^3 were punched in the plates. For each sample, the glass bead volume fraction was estimated accurately with an AccuPycII 1340 gas pycnometer. Three samples of both composites showing the targeted 55% volume fraction of glass fillers were selected. The samples were glued (with Loctite Flexcomet PU 15) to aluminum jaws and uniaxial tensile tests were carried out at the low constant crosshead speed of 0.1 mm/min on an Instron 5967 tensile machine. The strain was measured by video extensometry based on a Labview routine following two dots recorded by a 3 MPx camera equipped with a telecentric lens. The stress-strain responses of both composites are reported in Fig. 2a. Both materials display linear responses followed by some softening, a sign of the occurrence of some debonding at the matrix/filler interfaces for the matrix exhibits a rather linear behavior (Fig. 2b). However, while the softened response seems to remain stable up to failure for the composite filled with glass grits, a significant softening occurs at approximately 8% strain with a downturn followed by some hardening before failure for the beads composite. Additionally, the composite filled with polyhedral inclusions displays significantly larger strength but also more dispersion in the mechanical response. In order to understand the similarities and differences between the material responses, finite element analyses are now carried on numerical materials that are presented in the next section.

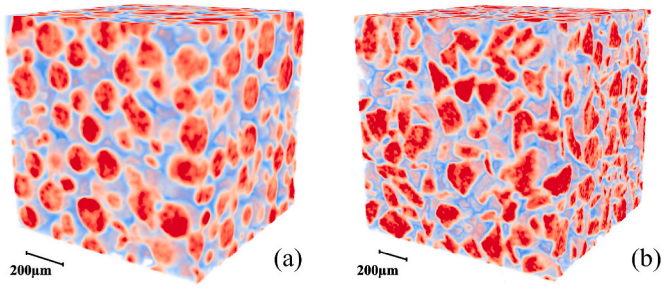

Fig. 1. μCT scans of model composites made of a methacrylate matrix highly filled with sifted glass beads (a) or glass slivers (b).

3. Numerical composites

3.1. Microstructure generation

3.1.1. Spherical inclusions

The complexity of generating isotropic materials when highly filled with monosized spheres lies in the difficulty to achieve high volume fractions while ensuring the random distribution of particles. Such microstructures have been extensively studied. The generation process detailed in Francqueville et al. (2019) has been reproduced directly here and only the main steps are recalled. A Lubachevsky and Stillinger (1990) algorithm was used (Skoge et al., 2006). In accordance with the literature (Gusev, 1997), periodic microstructures with 64 identical spheres have been generated and selected based on geometrical properties characterized thanks to the two-point correlation function and a nearest-neighbor distribution function. Note that during microstructure generations, the minimum distance between particles has not been restricted to avoid possible bias (Gusev, 2016).

3.1.2. Polyhedral inclusions

Microstructures defined by a matrix filled with randomly dispersed irregular polyhedra are obtained through a Voronoï tessellation, and the main steps of the generation process are illustrated in Fig. 3.

First, a microstructure with monosized spherical inclusions is generated. The centers of the spheres provide with a random dispersion of seed points with nearly the same surrounding volumes. In order to ensure periodicity, the set of seed points is temporarily duplicated 26 times around the original cell. Then the Delaunay tetrahedralization of the structure is computed and the vertices attached to each center are listed to compute the Voronoï diagram. This process leads to a complete filling of the volume. In order to reach the targeted volume fraction (55%) of fillers, a shrinking is applied to each polyhedron by shortening the segments linking its vertices to its seed point. At the end of this process, inspired by Fritzen and Boehlke (2009), such microstructures as shown in Fig. 4b are obtained. The volumes of irregular polyhedra present a dispersion of 10% around the mean volume and are mostly equiaxial with 14 faces on average. Hence, in order to ensure the exact same volume for every particle for a more rigorous comparison with microstructures filled with monosized spheres, the volume of each polyhedron was adjusted. Due to the shrinking process, and despite the irregular shape of the polyhedra, the distance between polyhedra is very regular and parallel planes are facing each other as it is visible in Fig. 3c. While this property is sometimes sought-after (Nadot-Martin et al., 2011), it is contradictory with the microstructure of actual composites, as one may see in Fig. 1. Therefore, the generation process has been complemented by applying random rotations and translations to each polyhedron. A random permutation of polyhedra indexes is defined and motions are applied sequentially according to the following sequences. Firstly, the type of perturbation, translation or rotation is randomly

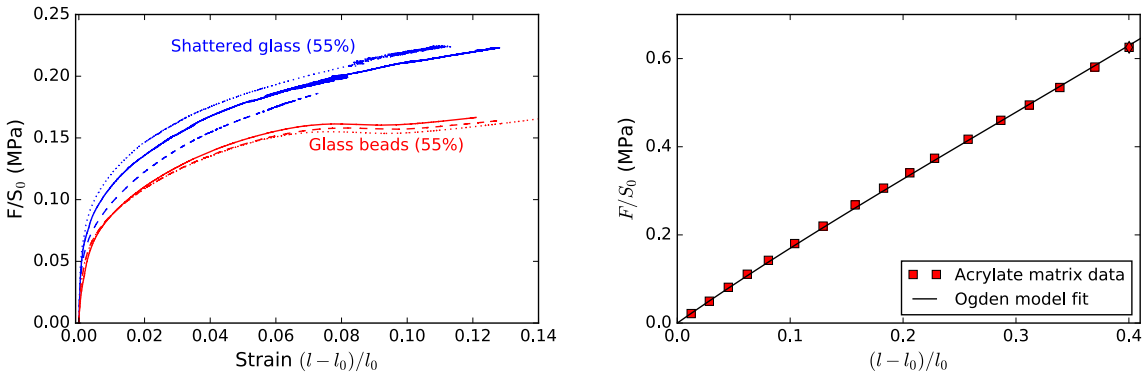

Fig. 2. (a) Uniaxial tensile responses recorded on three specimens for each model composite displayed in Fig. 1 and (b) the composite matrix behavior well reproduced by the hyperelastic Ogden model.

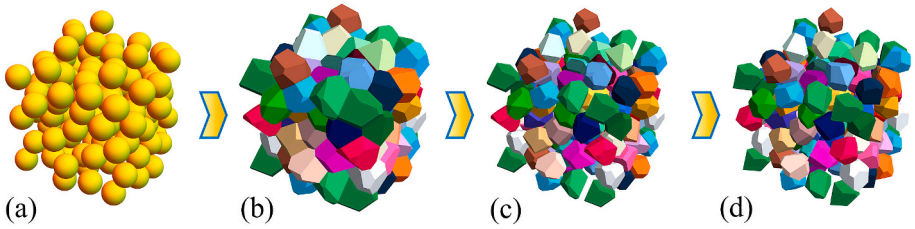

Fig. 3. Process of generation of a microstructure filled with randomly dispersed non-regular polyhedra, (a) starting with a random dispersion of spheres, (b) which centers are used as seed points for Voronï tessellation. (c) Then, particles are shrunk to lower the volume fraction of particles from 100 to 55%. (d) Finally, random rotations and translations are applied to each polyhedron.

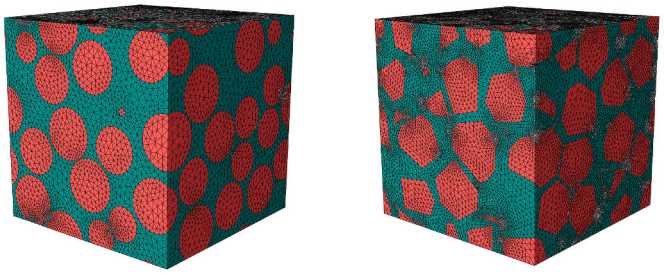

Fig. 4. Finite element meshes for periodic cells with 64 monosized spheres or polyhedra filling 55% volume of the microstructures.

chosen. Secondly, in the case of a rotation, a random rotation based on Euler angles weighted by an amplitude factor and centered on the seed point is set and applied to each vertex of the polyhedron. In the case of a translation, a random displacement vector is defined and weighted by another amplitude factor and applied to each vertex and to the seed point of the polyhedron. Thirdly, the transformation is validated or rejected, based on a polyhedra non-interpenetration criterion using the Gilbert-Johnson-Keerthie algorithm (Gilbert et al., 1988). When the random permutation list has been fully swept, each amplitude factor is increased if less than 50% of the transformations have been rejected, and decreased otherwise. Such a process is looped hundreds of times or until the amplitude factors reach a negligible threshold. It has to be applied with care to avoid periodicity loss on the cell. The whole procedure was implemented with Matlab (2017a) and takes about 1 h for generating one 64-particle microstructure on a basic laptop (2.59 GHz Intel Core i7-6700HQ CPU with 16 Go RAM), including a pre-meshing step that will be explained in the next section.

3.2. Framework of the numerical simulations

3.2.1. Microstructure meshing

A conformal mesh being required for finite element analyses, the free meshing software Netgen (Schöberl, 1997) is chosen for its efficiency to generate periodic meshes. It is also able to list the equations required by periodic boundary conditions in the format of the commercial finite element sofware Abaqus (2018) which is used here. In the case of spherical fillers, a local mesh refinement is implemented as visible in Fig. 4, in order to avoid excessively distorted elements in areas of near-to-touch spheres (Gusev, 2016).

Microstructures filled with polyhedra do not display exceedingly distorted elements. However, meshing failures have been detected as soon as a polyhedron vertex is at a distance smaller than a threshold of 10^{-4} times a, from any vertex, edge, or a face of a polyhedron or cell, a being the cell size. Therefore, a pre-meshing step has been added at the end of the generation procedure. For each polyhedron, internal distances (edge lengths) and the distances to all surrounding elements (cell faces, edges or corners, other polyhedron faces, edges or vertices) are estimated. If any internal length is smaller than the threshold, the corresponding edge is discarded by introducing an extra tiny face, following Quey et al. (2011). If any distance to a surrounding element is smaller than the threshold, very small random translations are tested until a valid position is obtained. The changes introduced during the pre-meshing step have been implemented with the constraint of microstructure periodicity. Finally, meshed microstructures such as shown in Fig. 4 are obtained.

3.2.2. Mechanical behavior

The fillers are made of glass, whose behavior may be defined as linear elastic characterized by a Young modulus of 69 GPa and a Poisson's ratio of 0.25, which are common values for glass. In order to better describe the polymer rubbery matrix behavior, it was subjected to uniaxial tensile tests. The non-linear stress-strain response was well

reproduced by the Ogden strain energy density (Ogden, 1972) with a single set of parameters, $\mu = 0.6$ MPa and $\alpha = 3.2$(Fig. 2b). Finally, a reasonable bulk modulus value of 3 GPa was chosen. Note that, due to the very large ratio of the bulk modulus over the shear modulus of the matrix, quadratic 10-node hybrid tetrahedral elements were used in this material phase, whereas standard quadratic 10-node tetrahedral elements were used in the glass particles.

Damage at the matrix/filler interfaces has been introduced thanks to CZM elements characterized by a simplified version of the Tvergaard and Hutchinson law (Tvergaard and Hutchinson, 1993) that is conveniently defined by three parameters only when normal and tangent interface behaviors are identical. The law is illustrated in Fig. 5, in the case of purely normal (or, equivalently, purely tangent) loading. Normal and shear cohesive stress constitutive equations write as,

$$\begin{cases} T_n = K\,\delta_n & \text{if } \delta_n < 0 \ \text{(compression)} \\ T_n = K\langle 1-D\rangle\delta_n & \text{if } \delta_n > 0 \\ \\ T_t = K\langle 1-D\rangle\delta_t \end{cases} \tag{1}$$

with the damage variable D defined as,

$$D = \frac{1}{\lambda^m}\frac{\langle \lambda^m - \frac{\delta^c}{\delta^f}\rangle}{1-\frac{\delta^c}{\delta^f}}, \quad \lambda^m = \max_t\left(\sqrt{\left(\frac{\langle\delta_n\rangle}{\delta^f}\right)^2 + \left(\frac{\delta_t}{\delta^f}\right)^2}\right) \tag{2}$$

with λ^m being the largest non-dimensional separation factor encountered at the interface. The Macaulay brackets, $\langle \bullet \rangle$, allow distinguishing normal separation from normal compression. Such cohesive elements are available in Abaqus for linear elements only. Therefore, in order to preserve consistency with the quadratic solid elements used in the mesh to ensure good convergence, quadratic cohesive elements have been implemented by writing a User Element routine.

The cohesive elements were inserted by duplicating all the facets at the surfaces of the fillers and by creating quadratic 12-node prismatic cohesive elements with null initial thicknesses. This duplication process takes into account the periodic equations for nodes located on the sides of the microstructure cell. Finally, dummy 6-node triangular elements were defined on the particles surfaces to allow the visualization of the damage state in the cohesive elements, which was passed on to the dummy elements via a UVARM user routine. To make the influence of the dummy elements negligible, their Young modulus was set to 10^{-20} MPa with a Poisson's ratio of 0.25.

Note that a viscous regularization was introduced to improve the computational convergence, adapting the method of Gao and Bower (2004) to the Tvergaard and Hutchinson law. The negligible impact of the viscous term on the computed mechanical response has been verified, while its efficiency allowed to delay the computational divergence significantly.

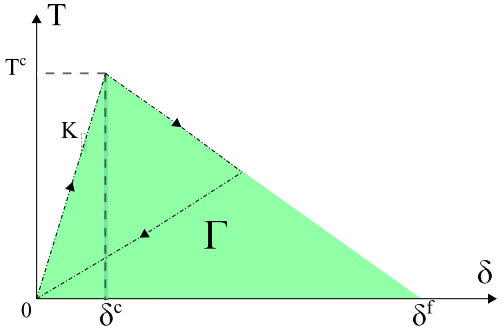

Fig. 5. Cohesive elements traction-separation behavior for a purely normal (or purely tangent) displacement that may be characterized by three independent parameters among the set of five (K, Γ, T^c, δ^c, δ^f).

4. Results and discussion

4.1. Macroscopic stress-strain responses of numerical composites

In order to validate the reproducibility of the obtained numerical results, some simulations were run with the same set of parameters for two different microstructures filled with polyhedra. Fig. 6 shows the numerical macroscopic responses. Firstly, the isotropy of one microstructure is confirmed. Secondly, the macroscopic responses of two different microstructures are very similar. This will allow us to look at the response of one microstructure in one direction only.

The macroscopic behaviors and local damages of microstructures filled with monosized spheres have been studied before (de Francqueville et al., 2020). Therefore three sets of parameters, listed in Table 1, have been carefully selected for their displacements to failure δ^f consistent with the size of the particles, and critical strengths T^c driving to different microstructure failure scenarii.

Simulations were run on both kinds of microstructures. Fig. 7 shows the macroscopic responses obtained for the three sets of CZM parameters that are also displayed. According to the CZM parameters, three types of behaviors are obtained but similar stress-strain responses are shown for both types of reinforcements. In case 1, the linear elastic response is followed by a steady softening. This behavior shows the same features as the actual composites filled with grits. In case 2, after the softening sets in, a downturn appears which is a feature that is witnessed on the actual composite filled with spheres (Fig. 2). Finally, in case 3, damage appears earlier, which is understandable due to a lower value of T^c. While the composite strength is low the softening is steady like in case 2. More importantly, according to the numerical results, the faceted particles do not seem to change significantly the macroscopic results of the composites, and the difference of behaviors witnessed in Fig. 2 for the actual materials is likely due to a change in the matrix/filler interface properties rather than in the shape of the fillers. To better understand the similarities of the macroscopic behaviors, a close look is taken at the local damage undergone at the filler interfaces.

4.2. Local damage initiation and evolution upon stretching

The analysis of the local damage characterized by the matrix debonding at the filler/matrix interfaces provides with a local understanding of the macroscopic behavior. Starting with case 1, at the beginning of the loading, when the material response is linear, no CZM element has reached the critical strength T^c, then the macroscopic

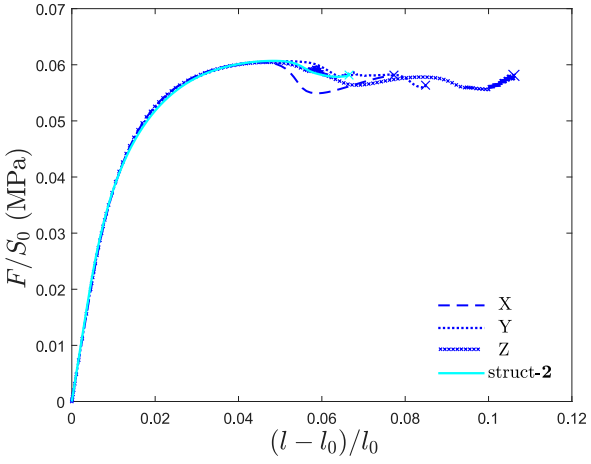

Fig. 6. Comparison between the stress-strain responses of one polyhedra microstructure submitted to uniaxial tension according to each Cartesian axis and another polyhedra microstructure. Symbols designate the computational divergence.

Table 1
Cohesive-zone properties for which the numerical responses are computed and analyzed.

	K (MPa/mm)	T^c (MPa)	δ^f (mm)
Case 1	70	0.05	0.02
Case 2	70	0.1	0.02
Case 3	70	0.1	0.06

softening results from damage occurring on several elements where T^c has been reached. The low value of T^c favors the early development of damage evenly spread across the microstructure resulting in the low stress-strain response. At larger strain, complete matrix/filler separation appears on several elements across the microstructure as one can read in Fig. 8. In case 2, material macroscopic stress-strain response softens when damage occurs at the matrix/filler interface. Later, the downturn happens when several CZM elements, located in a plane perpendicular to the direction of applied tension, reach δ^f that is complete failure (Fig. 8). It is worth noting that once localization happens, it may be enhanced by the periodic boundary conditions. Therefore, results will not be discussed passed the localization appearance. In case 3, damage evolves slowly without reaching complete failure due to the large value of δ^f.

As shown in Fig. 8, the same types of damage are witnessed for both types of microstructures, explaining the similar stress-strain responses displayed in Fig. 7. The fact that the microstructure filled with spherical particles shows stress-strain responses slightly below the stress-strain responses of the polyhedra filled microstructure is more likely due to the early appearance of damage where particles are close to touch in the microstructure with spherical particles. Actually, two very close spherical particles create very strong stress concentration. This was not necessarily witnessed in previous studies due to lower volume fractions of particles or due to a prescribed minimum distance between particles.

These results prove that for highly filled rubberlike materials,

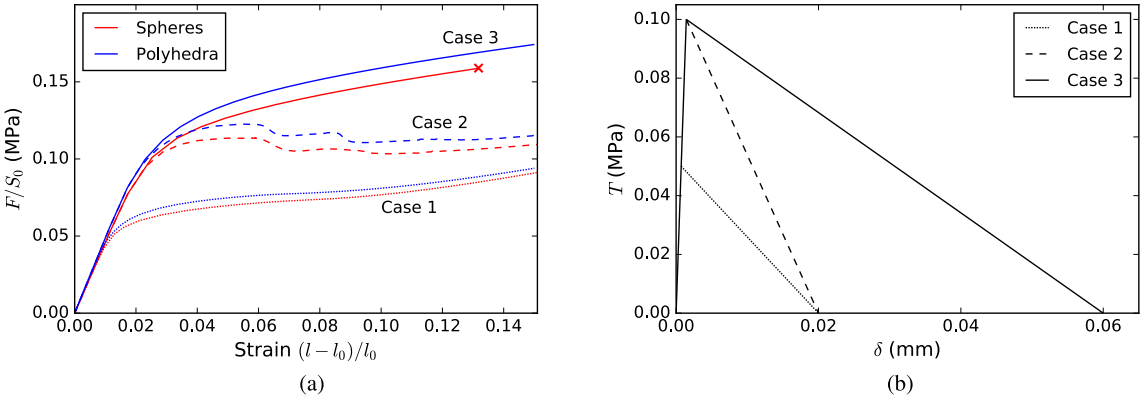

Fig. 7. (a) Macroscopic stress-strain responses of microstructures filled with polyhedra or spheres for (b) the cohesive-zone parameters listed in Table 1. Computational divergence are indicated by a cross symbol.

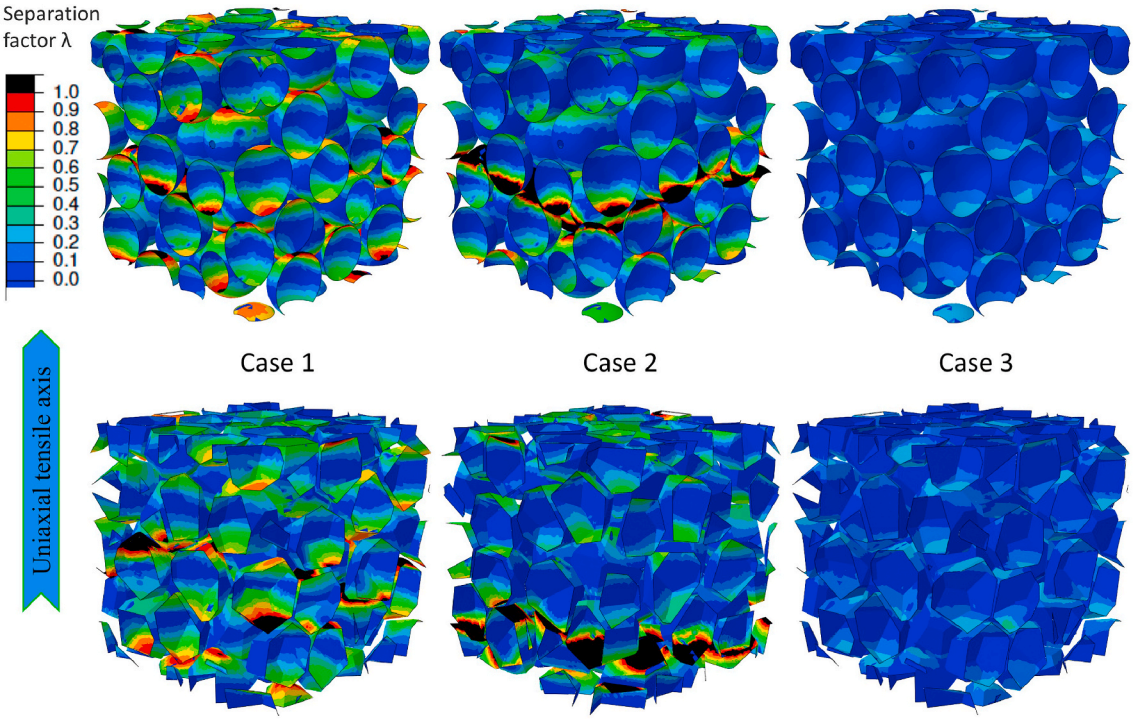

Fig. 8. Maps of the interface separation factor at 8% macroscopic strain in microstructures filled with spheres (top) or polyhedra (bottom) for the three sets of cohesive-zone parameters listed in Table 1.

polyhedral particles are not more critical than spheres for the appearance and development of damage at their surfaces, as one could have wrongly anticipated. Actually, the shape of the composite stress-strain response appears to be driven more by the properties of the filler/matrix interface than by the shape of the fillers. Coming back to the experimental behaviors presented in Fig. 2, one would identify the behavior of the glass beads composite with the responses of case 2, and the glass grits composite with case 3. According to our simulations, the difference in behaviors between the two materials is not to be explained by different particle shapes but rather by different adhesion properties at the matrix/filler interfaces due to different types of glass and/or different fillers roughnesses.

5. Conclusions

The influence of the fillers shape on the finite strain behavior of highly filled composites (>50%) has been examined through micromechanical finite element simulations accounting for damage with a cohesive-zone model. This analysis has been motivated by the uniaxial responses of two actual materials filled with either sifted glass beads or sifted glass grits. While the generation of microstructures highly filled with a random dispersion of monosized spheres is available in the literature, an original generation process has been developed to obtain periodic random dispersions of monosized polyhedra. This process includes a Voronoï tessellation, a shrinkage of all polyhedra, and application of random rotations and translations to each polyhedron to ensure a representative configuration of the fillers. Damage has been introduced accounting for debonding at the matrix/filler interface with a cohesive zone model. When simulating the mechanical behavior of the numerical composites with finite element analyses, a second order influence of fillers shape on the composite behavior has been observed, with only a slight delay of damage initiation in the case of polyhedral fillers. The local damage fields have exhibited the same trends for both particles shapes, for different matrix/filler interface behaviors. Results show that for highly filled rubberlike materials near-to-touch spherical particles are sources of stress concentrations that favor early damage appearance. The different behaviors observed on actual composites are therefore assumed to result from different adhesion properties between fillers and matrix, probably due to different types of glass or/and different fillers roughnesses.

Declaration of competing interest

The authors declare that they have no known competing financial interests or personal relationships that could have appeared to influence the work reported in this paper.

Acknowledgements

Acquisition of the microtomography device of laboratoire Navier (ENPC) has been made possible thanks to grants from the Région Ile-de-France (SESAME 2007 program) and CNRS. This work was supported by the ANR under contract number ANR-10-EQPX- 37, and the authors thank the Délégation Générale de l'Armement (DGA) and ArianeGroup, Vert-le-Petit (France), for their financial supports.

References

Abaqus, 2018. Abaqus Standard Version 2018. Dassault Systèmes Simulia Corp.

Böhm, H.J., Rasool, A., 2016. Effects of particle shape on the thermoelastoplastic behavior of particle reinforced composites. Int. J. Solid Struct. 87, 90–101. https://doi.org/10.1016/j.ijsolstr.2016.02.028.

Caballero, A., López, C.M., Carol, I., 2006. 3D meso-structural analysis of concrete specimens under uniaxial tension. Comput. Methods Appl. Mech. Eng. 195, 7182–7195. https://doi.org/10.1016/j.cma.2005.05.052.

Carol, I., Idiart, A., Lopez, C.M., Caballero, A., 2007. Advances in Meso-Mechanical Analysis of Concrete Specimens Using Zero-Thickness Interface Elements. FraMCoS-6th, pp. 163–174.

Cornwell, L.R., Schapery, R.A., 1975. SEM study of microcracking in strained solid propellant. Metallography 8, 445–452. https://doi.org/10.1016/0026-0800(75)90013-0.

Cras, J.J., Rowe-Taitt, C.A., Nivens, D.A., Ligler, F.S., 1999. Comparison of chemical cleaning methods of glass in preparation for silanization. Biosens. Bioelectron. 14, 683–688. https://doi.org/10.1016/S0956-5663(99)00043-3.

Drach, B., Tsukrov, I., Trofimov, A., 2016. Comparison of full field and single pore approaches to homogenization of linearly elastic materials with pores of regular and irregular shapes. Int. J. Solid Struct. 96, 48–63. https://doi.org/10.1016/j.ijsolstr.2016.06.023.

de Francqueville, F., Gilormini, P., Diani, J., 2019. Representative volume elements for the simulation of isotropic composites highly filled with monosized spheres. Int. J. Solid Struct. 158, 277–286. https://doi.org/10.1016/j.ijsolstr.2018.09.013.

de Francqueville, F., Gilormini, P., Diani, J., Vandenbroucke, A., 2020. Relationship between local damage and macroscopic response of soft materials highly reinforced by monodispersed particles. Mech. Mater. https://doi.org/10.1016/j.mechmat.2020.103408.

Fritzen, F., Boehlke, T., Schnack, E., 2009. Periodic three-dimensional mesh generation for crystalline aggregates based on Voronoi tessellations. Comput. Mech. 43, 701–713. https://doi.org/10.1007/s00466-008-0339-2.

Fritzen, F., Boehlke, T., 2011. Periodic three-dimensional mesh generation for particle reinforced composites with application to metal matrix composites. Int. J. Solid Struct. 48, 706–718. https://doi.org/10.1016/j.ijsolstr.2010.11.010.

Gao, Y.F., Bower, A.F., 2004. A simple technique for avoiding convergence problems in finite element simulations of crack nucleation and growth on cohesive interfaces. Model. Simulat. Mater. Sci. Eng. 12, 453–463. https://doi.org/10.1088/0965-0393/12/3/007.

Gilbert, E.G., Johnson, D.W., Keerthi, S.S., 1988. A fast procedure for computing the distance between complex objects in three-dimensional space. IEEE J. Robot. Autom. 4, 193–203. https://doi.org/10.1109/56.2083.

Gilormini, P., Toulemonde, P.A., Diani, J., Gardere, A., 2017. Stress-strain response and volume change of a highly filled rubbery composite: experimental measurements and numerical simulations. Mech. Mater. 111, 57–65. https://doi.org/10.1016/j.mechmat.2017.05.006.

Gusev, A., 1997. Representative volume element size for elastic composites: a numerical study. J. Mech. Phys. Solid. 45, 1449–1459. https://doi.org/10.1016/S0022-5096(97)00016-1.

Gusev, A., 2016. Controlled accuracy finite element estimates for the effective stiffness of composites with spherical inclusions. Int. J. Solid Struct. 80, 227–236. https://doi.org/10.1016/j.ijsolstr.2015.11.006.

Inglis, H.M., Geubelle, P.H., Matouš, K., Tan, H., Huang, Y., 2007. Cohesive modeling of dewetting in particulate composites: micromechanics vs. multiscale finite element analysis. Mech. Mater. 39, 580–595. https://doi.org/10.1016/j.mechmat.2006.08.008.

Kanit, T., Forest, S., Galliet, I., Mounoury, V., Jeulin, D., 2003. Determination of the size of the representative volume element for random composites: statistical and numerical approach. Int. J. Solid Struct. 40, 3647–3679. https://doi.org/10.1016/S0020-7683(03)00143-4.

Lavergne, F., Sab, K., Sanahuja, J., Bornert, M., Toulemonde, C., 2015. Investigation of the effect of aggregates' morphology on concrete creep properties by numerical simulations. Cement Concr. Res. 71, 14–28. https://doi.org/10.1016/j.cemconres.2015.01.003.

Li, G., Wang, Y., Jiang, A., Yang, M., Li, J., 2018. Micromechanical investigation of debonding processes in composite solid propellants. Propellants, Explos. Pyrotech. 43, 642–649. https://doi.org/10.1002/prep.201700199.

LLorca, J., Segurado, J., 2004. Three-dimensional multiparticle cell simulations of deformation and damage in sphere-reinforced composites. Mater. Sci. Eng. A365, 267–274. https://doi.org/10.1016/j.msea.2003.09.035.

Lubachevsky, B.D., Stillinger, F.H., 1990. Geometric properties of random disk packings. J. Stat. Phys. 60, 561–583. https://doi.org/10.1007/BF01025983.

Matlab, 2017. Matlab 2017a. MathWorks Inc.

Moraleda, J., Segurado, J., LLorca, J., 2009. Effect of interface fracture on the tensile deformation of fiber-reinforced elastomers. Int. J. Solid Struct. 46, 4287–4297. https://doi.org/10.1016/j.ijsolstr.2009.08.020.

Nadot-Martin, C., Halm, D., Dartois, S., Touboul, M., Dragon, A., Fanget, A., 2011. Une approche multi-échelles directe pour modéliser le comportement non linéaire des composites énergétiques. JNC-17th, p. 204.

Oberth, A.E., Bruenner, R.S., 1965. Tear phenomena around solid inclusions in castable elastomers. Trans. Soc. Rheol. 9, 165–185. https://doi.org/10.1122/1.548997.

Ogden, R.W., 1972. Large deformation isotropic elasticity - on the correlation of theory and experiment for incompressible rubberlike solids. Proc. Roy. Soc. Lond. A326, 565–584. https://doi.org/10.1098/rspa.1972.0026.

Quey, R., Dawson, P.R., Barbe, F., 2011. Large-scale 3D random polycrystals for the finite element method: generation, meshing and remeshing. Comput. Methods Appl. Mech. Eng. 200, 1729–1745. https://doi.org/10.1016/j.cma.2011.01.002.

Schöberl, J., 1997. Netgen an advancing front 2D/3D-mesh generator based on abstract rules. Comput. Visual Sci. 1, 41–52. https://doi.org/10.1007/s007910050004.

Segurado, J., LLorca, J., 2005. A computational micromechanics study of the effect of interface decohesion on the mechanical behavior of composites. Acta Mater. 53, 4931–4942. https://doi.org/10.1016/j.actamat.2005.07.013.

Sheng, P., Zhang, J., Ji, Z., 2016. An advanced 3D modeling method for concrete-like particle-reinforced composites with high volume fraction of randomly distributed particles. Compos. Sci. Technol. 134, 26–35. https://doi.org/10.1016/j.compscitech.2016.08.009.

Skoge, M., Donev, A., Stillinger, F.H., Torquato, S., 2006. Packing hyperspheres in high-dimensional Euclidean spaces. Phys. Rev. E 74, 041127. https://doi.org/10.1103/PhysRevE.74.041127.

Toulemonde, P.A., Diani, J., Gilormini, P., Desgardin, N., 2016. On the account of a cohesive interface for modeling the behavior until break of highly filled elastomers. Mech. Mater. 93, 124–133. https://doi.org/10.1016/j.mechmat.2015.09.014.

Tvergaard, V., Hutchinson, J.W., 1993. The influence of plasticity on mixed mode interface toughness. J. Mech. Phys. Solid. 41, 1119–1135. https://doi.org/10.1016/0022-5096(93)90057-M.

Weng, L., Fan, T., Wen, M., Shen, Y., 2019. Three-dimensional multi-particle FE model and effects of interface damage, particle size and morphology on tensile behavior of particle reinforced composites. Comput. Struct. 209, 590–605. https://doi.org/10.1016/j.compstruct.2018.11.008.

Widom, B., 1966. Random sequential addition of hard spheres to a volume. J. Chem. Phys. 44, 3888–3894. https://doi.org/10.1063/1.1726548.

Williams, J.J., Segurado, J., Llorca, J., Chawla, N., 2012. Three dimensional (3D) microstructure-based modeling of interfacial decohesion in particle reinforced metal matrix composites. Mater. Sci. Eng. A 557, 113–118. https://doi.org/10.1016/j.msea.2012.05.108.

Wimmer, J., Stier, B., Simon, J.W., Reese, S., 2016. Computational homogenisation from a 3D finite element model of asphalt concrete linear elastic computations. Finite Elem. Anal. Des. 110, 43–57. https://doi.org/10.1016/j.finel.2015.10.005.

Zhang, B., Yiu, X., Gu, B., 2018. Modeling and experimental validation of interfacial fatigue damage in fiber-reinforced rubber composites. Polym. Eng. Sci. 58, 920–927. https://doi.org/10.1002/pen.24646.